A system for imaging the regulatory noncoding *Xist* RNA in living mouse embryonic stem cells

Karen Ng[a], Nathalie Daigle[b], Aurélien Bancaud[c,d], Tatsuya Ohhata[e], Peter Humphreys[e], Rachael Walker[e], Jan Ellenberg[b], and Anton Wutz[a,e]

[a]Research Institute of Molecular Pathology, 1030 Vienna, Austria; [b]Cell Biology and Biophysics Unit, European Molecular Biology Laboratory, 69117 Heidelberg, Germany; [c]Laboratoire d'Analyse et d'Architecture des Systèmes, Centre National de la Recherche Scientifique, F-31077 Toulouse, France; [d]Université Toulouse III–Paul Sabatier, Institut National des Sciences Appliquées, Institut National Polytechnique, Institut Supérieur de l'Aéronautique et de l'Espace, and Laboratoire d'Analyse et d'Architecture des Systèmes, F-31077 Toulouse, France; [e]Wellcome Trust Centre for Stem Cell Research, Cambridge CB2 1QR, United Kingdom

ABSTRACT **In mammals, silencing of one of the two X chromosomes in female cells compensates for the different number of X chromosomes between the sexes. The noncoding *Xist* RNA initiates X chromosome inactivation. *Xist* spreads from its transcription site over the X chromosome territory and triggers the formation of a repressive chromatin domain. To understand localization of *Xist* over one X chromosome we aimed to develop a system for investigating *Xist* in living cells. Here we report successful visualization of transgenically expressed MS2-tagged *Xist* in mouse embryonic stem cells. Imaging of *Xist* during an entire cell cycle shows that *Xist* spreads from a single point to a steady state when the chromosome is covered with a constant amount of *Xist*. Photobleaching experiments of the established *Xist* cluster indicate that chromosome-bound *Xist* is dynamic and turns over on the fully *Xist* covered chromosome. It appears that in interphase the loss of bound *Xist* and newly produced *Xist* are in equilibrium. We also show that the turnover of bound *Xist* requires transcription, and *Xist* binding becomes stable when transcription is inhibited. Our data reveal a strategy for visualizing *Xist* and indicate that spreading over the chromosome might involve dynamic binding and displacement.**

Monitoring Editor
A. Gregory Matera
University of North Carolina

Received: Feb 25, 2011
Revised: Apr 19, 2011
Accepted: May 16, 2011

INTRODUCTION

In mammals the dosage difference that arises from the different number of X chromosomes between the sexes is compensated by X inactivation (Heard and Disteche, 2006; Payer and Lee, 2008). Early in female development one of the two X chromosomes is selected for inactivation in a random manner. This process involves counting the number of X chromosomes, choosing which chromosome to inactivate, and keeping the other X active in a reciprocal manner (Minks and Brown, 2009; Barakat *et al.*, 2010). Chromosome-wide inactivation of one X chromosome requires the noncoding *Xist* RNA (Borsani *et al.*, 1991; Brockdorff *et al.*, 1991; Brown *et al.*, 1991a, 1991b). *Xist* is expressed from the future inactive X chromosome (Xi) and spreads over the X chromosome territory (Clemson *et al.*, 1996). Thereby, *Xist* serves as a paradigm for studying noncoding RNA function in regulating chromatin organization.

The process of random X inactivation is recapitulated during the differentiation of female mouse embryonic stem (ES) cells. ES cells have therefore been extensively used for studying the mechanism of *Xist* function. Accumulation of *Xist* over the chromosome leads to the exclusion of RNA polymerase II and factors associated with transcription and splicing from the X chromosome nuclear domain (Okamoto *et al.*, 2004; Chaumeil *et al.*, 2006). Loss of activating histone modifications and recruitment of Polycomb group complexes lead to the formation of a repressive compartment (Chaumeil *et al.*, 2002, 2006). Subsequently, chromatin modifications, including trimethylation of histone H3 lysine 27 and ubiquitination of histone H2A, contribute to the establishment of facultative heterochromatin on the Xi (Heard and Bickmore, 2007). It has been shown that the formation of a repressive compartment can be separated

This article was published online ahead of print in MBoC in Press (http://www.molbiolcell.org/cgi/doi/10.1091/mbc.E11-02-0146) on May 25, 2011.

Address correspondence to: Anton Wutz (aw512@cam.ac.uk) or Jan Ellenberg (jan.ellenberg@embl.de).

Abbreviations used: Dox, doxycycline; ES, embryonic stem; FCS, fluorescence correlation spectroscopy; FRAP, fluorescence recovery after photobleaching; GFP, green fluorescent protein; Xi, inactive X chromosome.

from gene silencing by specific mutations within *Xist*. The 5′ end of *Xist* that contains the repeat A sequence motif is required for gene repression (Wutz *et al.*, 2002). Expression of *Xist* with a mutation of repeat A leads to the formation of a repressive compartment without initiation of gene repression (Chaumeil *et al.*, 2006; Pullirsch *et al.*, 2010). Recruitment of genes to the repressive compartment requires repeat A and involves additional pathways (Blewitt *et al.*, 2008; Agrelo *et al.*, 2009). From these observations it is clear that localization of *Xist* over the X chromosome does not require gene silencing. Consistent with this, previous studies have observed that expression of *Xist* in most differentiated cells does not lead to the initiation of gene silencing, whereas *Xist* RNA localization appears normal (Beard *et al.*, 1995; Wutz and Jaenisch, 2000; Sado *et al.*, 2004; Savarese *et al.*, 2006).

Xist localization is not dependent on an X chromosomal context. Using transgenes, it has been shown that *Xist* can spread in *cis* over autosomes and cause repression of at least certain autosomal genes (Lee *et al.*, 1996; Herzing *et al.*, 1997; Heard *et al.*, 1999; Wutz and Jaenisch, 2000; Hall *et al.*, 2002; Chow *et al.*, 2007; Tang *et al.*, 2010). This suggests that X chromosome specific–sequences are not crucial for attachment of *Xist* to the chromosome. However, analysis of translocation chromosomes indicates that the X chromosome might be more permissive for *Xist* spreading (Popova *et al.*, 2006). In interphase *Xist* localizes to the core of the X chromosome territory that is composed of mainly noncoding sequences and genomic repeats (Chaumeil *et al.*, 2006; Clemson *et al.*, 2006). In particular, long interspersed elements (LINEs) have been implicated in X inactivation (Lyon, 2003; Tang *et al.*, 2010). Taken together, these findings suggest that *Xist* might initially attach to genomic repeat sequences. *Xist* has also been shown to be retained in the nuclear matrix when chromatin is extracted (Clemson *et al.*, 1996). The ability of *Xist* to attach to the nuclear matrix has led to the proposal that *Xist* performs a structural role associated with the stability of the Xi territory. Consistent with this idea, chromosomal binding of *Xist* has been shown to be stable with a half-life of between 4 and 8 h when transcription is blocked (Panning *et al.*, 1997; Wutz and Jaenisch, 2000; Sun *et al.*, 2006). *Xist* localization requires the scaffold attachment factor A (SAF-A) gene (Hasegawa *et al.*, 2010). SAF-A has been shown to be associated with the Xi nuclear matrix and contributes to a stable nuclear structure of the Xi in somatic cells (Helbig and Fackelmayer, 2003). The binding of SAF-A on the Xi has been measured under conditions that do not block transcription and shown to be statically bound with a half-life of over hours (Fackelmayer, 2005). The apparent static binding of *Xist* and SAF-A to the Xi raises the question of how *Xist* is distributed from the *Xic* locus over the chromosome territory.

Here we describe a new tool for studying *Xist* dynamics and apply it to investigate the mechanism of *Xist* spreading. By visualizing the noncoding RNA in living mouse embryonic stem cells, we present data indicating that *Xist* dynamically associates with the chromosome.

RESULTS

In vivo labeling of *Xist* RNA in embryonic stem cells

To visualize *Xist* RNA in living cells, we chose a system for fluorescently labeling RNA in vivo. For this we adopted a strategy of tagging *Xist* with an RNA motif from the MS2 phage that can be bound by an MS2 RNA-binding protein. This system has been used extensively in imaging cellular RNAs in a variety of organisms (Bertrand *et al.*, 1998; Fusco *et al.*, 2003, 2004; Janicki *et al.*, 2004). A U-to-C mutation in this RNA sequence (C-variant) has been identified that interacts much more strongly with the MS2-binding protein and forms a complex with picomolar binding affinity (Lowary and Uhlenbeck, 1987). We introduced 24 C-variant MS2-binding sites (5′-ACAUGAGGAUCACCCAUGU-3′) at the 3′ end of *Xist* (*Xist*-MS2). For regulating *Xist*-MS2 expression we used a tetracycline-inducible promoter. Similar transgenes have been shown previously to recapitulate silencing on autosomes in male mouse ES cells (Wutz and Jaenisch, 2000; Tang *et al.*, 2010). The *Xist*-MS2 transgene was introduced into J1:R26/N-nlsrtTA ES cells (Wutz and Jaenisch, 2000), which contained a tetracycline-inducible transactivator expressed from the ubiquitous *ROSA26* locus (Figure 1A). Subsequently a transgene for expression in the MS2 RNA-binding protein green fluorescent protein (GFP) fusion (MCP-GFP) (Bertrand *et al.*, 1998; Fusco *et al.*, 2003, 2004; Janicki *et al.*, 2004) was introduced into these XM ES cells (Figure 1B). The resulting XMG ES cells contained seven copies of the *Xist*-MS2 transgene integrated into a single site in the distal third of chromosome 7 (Figure 1, C–E).

We verified *Xist* expression by RNA fluorescence in situ hybridization (FISH) analysis using probes specific for *Xist* and MS2 sequences. *Xist*-MS2 accumulated in the vicinity of its transcription site upon induction of expression with doxycycline (Dox; Figure 1F). Importantly, the *Xist* domain could also be observed by immunostaining with an antibody detecting the RNA-binding MCP-GFP fusion protein in XMG ES cells, showing that the MS2 RNA tag on *Xist*-MS2 was recognized by the MS2 RNA-binding protein in living cells (Figure 1G).

To determine whether the MS2-modified *Xist* retained its function, we performed an analysis of chromatin modifications. We observed trimethylation of histone H3 lysine 27 and mono-ubiquitination of histone H2A lysine 119 overlapping the *Xist*-MS2 domain, demonstrating that transgenic *Xist*-MS2 expression led to epigenetic marks that are associated with X inactivation (Figure 1H). To further assess gene silencing in the autosomal context, we analyzed the expression of several imprinted genes on chromosome 7. Imprinted genes are expressed from one of the parental chromosomes, and therefore repression of genes that are expressed from the *Xist*-MS2 transgenic chromosome can be measured. We observed repression of the paternally expressed imprinted *Peg3*, *Snrpn*, and *Ndn* genes on chromosome 7 upon *Xist* induction (Figure 1I). In contrast the maternally expressed imprinted *H19* gene was not changed upon induction, suggesting that the *Xist*-MS2 transgene had integrated into the paternally inherited chromosome. *Xist*-MS2 induction caused strong repression of *Snrpn* and weaker repression of *Peg3*. *Ndn* was slightly repressed. Our data show that *Xist*-MS2 represses autosomal genes to various degrees. This is consistent with a recent study that comprehensively analyzed gene repression by autosomal *Xist* transgenes (Tang *et al.*, 2010). Taken together, our observations show that *Xist*-MS2 retains several aspects of *Xist* function in an autosomal context.

Analysis of *Xist* localization during the cell cycle

We next attempted to image *Xist* in living cells. A clearly defined green fluorescent territory was observed in the nucleus of living XMG ES cells after induction with Dox (Figure 2A). The fluorescence signal was low and required optimizing of the imaging conditions to avoid photobleaching. Using a confocal microscope that had been previously optimized for GFP imaging, we were able to capture a z-stack of images at high resolution under low excitation levels. Three-dimensional (3D) reconstruction of confocal images revealed a high density of *Xist* in the center and small clusters in the periphery of the *Xist* domain, which might reflect a heterogeneous distribution of *Xist* on the chromosome (Figure 2B and Supplemental Movie 1).

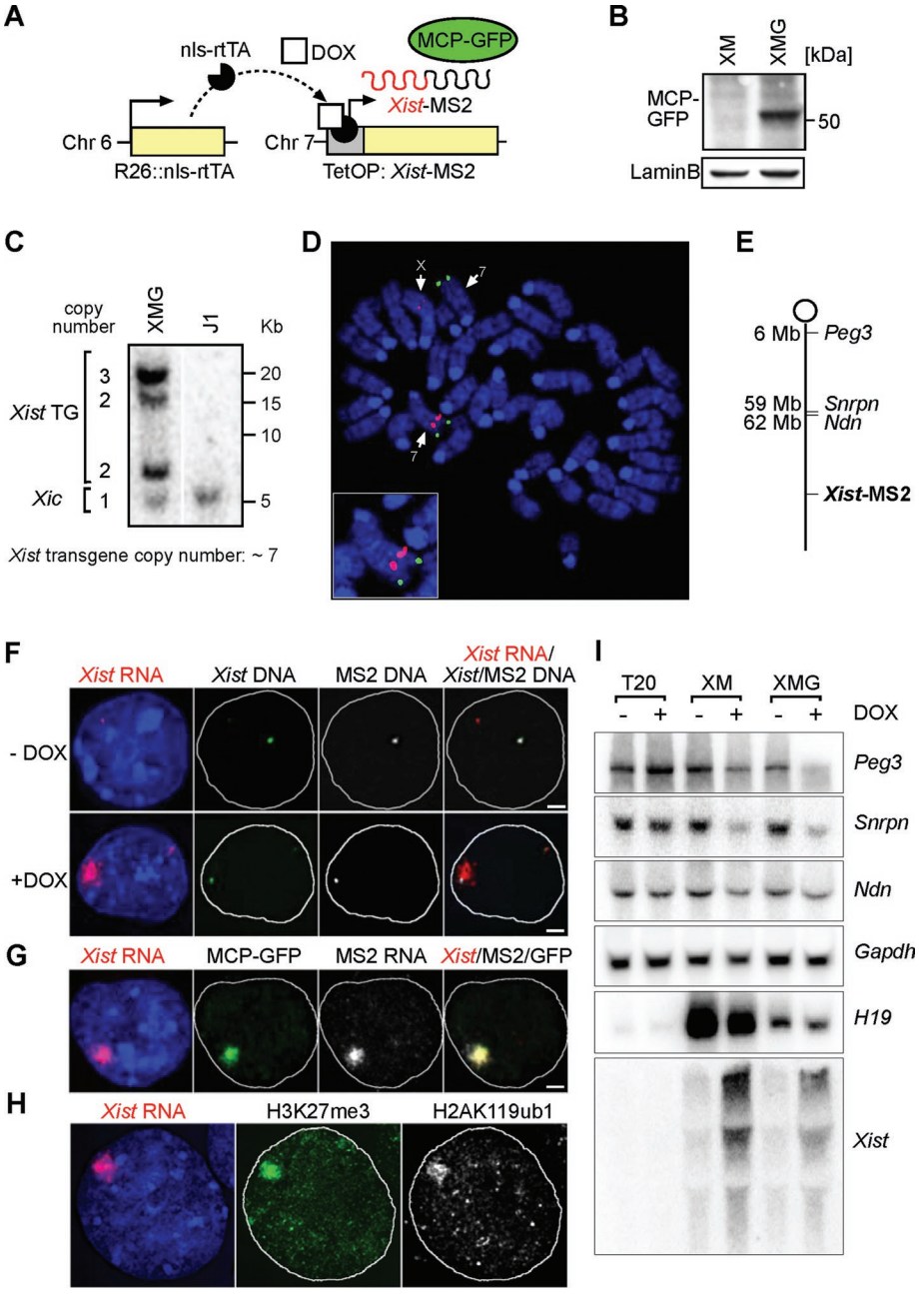

FIGURE 1: Visualization of *Xist* in living XMG ES cells. (A) In XMG ES cells, expression of *Xist*-MS2 can be induced from a tetracycline-inducible promoter (TetOP) with Dox. The green fluorescent MCP-GFP RNA-binding protein is recruited to the MS2 sequences on the 3′ end of *Xist*-MS2. (B) Western analysis detects MCP-GFP expression in nuclear extracts from XMG ES cells. Lamin B is a loading control. (C) Southern analysis of XMG ES cells using the XB1K probe specific for *Xist* exon 1. Band intensities were quantified relative to the endogenous *Xist* gene in the *Xic*. An estimate of seven transgene copies is calculated. (D) Mapping of the *Xist*-MS2 transgene integration site to chromosome 7. A DNA FISH experiment on a metaphase spread from XMG ES cells using an *Xist* probe recognizing the endogenous *Xist* locus and transgene (red) and an Igf2/H19 BAC (RP23-50N22) FISH probe identifying chromosome 7 (green) is shown. (E) A map of the transgenic chromosome 7 in XMG ES cells. (F) Sequential RNA/DNA FISH of XMG ES cells using probes specific for *Xist* RNA (red), *Xist* DNA (green), and MS2 DNA (white) after 2 d of Dox addition (+DOX) or without induction (−DOX). Nucleus is stained with DAPI (blue). Scale bar, 2 μm. (G) Colocalization of GFP signal with *Xist* RNA demonstrated by combined GFP immunofluorescence and RNA FISH detecting MS2 (white) and *Xist* (red) in XMG ES cells 2 d after Dox addition. Scale bars, 2 μm. (H) Transgenic *Xist* expression induces histone modifications in XMG ES cells. Combined immunofluorescence RNA FISH analysis shows colocalization of H3K27me3 (green), H2AK119ub1 (white), and *Xist* RNA (red) in XMG ES cells after 2 d of Dox addition. (I) *Xist* expression in XM and XMG cells causes gene silencing on chromosome 7. Northern analysis of *Xist* and the imprinted and paternally expressed genes *Peg3*, *Snrpn*, and *Ndn* in control T20 (Schoeftner *et al.*, 2006), XM, and XMG cells differentiated for 4 d in the presence (+) and absence (−) of Dox. The maternally expressed imprinted *H19* gene is not repressed upon *Xist* induction but is expressed at variable levels in different ES cell lines. *Gapdh* is a loading control.

To analyze spreading of *Xist* RNA, we used time-lapse confocal microscopy. Adjusting imaging conditions for recording multiple z series without significant bleaching allowed recording at a fairly high resolution. First, we studied *Xist* localization after initial induction with Dox in interphase (Figure 3A). *Xist* first appeared as a single diffraction-limited focus of <0.5 μm^2, which progressively expanded, reaching an area of 4.3 ± 0.8 μm^2 within ~1.5 h (Figure 3C). This expansion seemed to result from the binding of additional *Xist* molecules to a larger area, as the local concentration of *Xist* remained constant (Figure 3D). During the expansion of the *Xist*-covered area, the number of *Xist* molecules increased and reached a stable level within ~1.5 h as judged by the total fluorescence intensity of the domain (Figure 3D). Our observations give a first indication of the time scale for the spreading of *Xist* and suggest that a significant amount of time is required to accumulate *Xist* RNA over the chromosome territory.

Xist dissociated from the chromosome when the cells entered into mitosis (Figure 3B). After cell division *Xist* reappeared as a spot under conditions at which *Xist*-MS2 expression was continuously induced with Dox. We measured the reappearance of *Xist* after mitosis (Figure 3B). Strikingly, the kinetics of *Xist* accumulation after initial induction in interphase and during postmitotic reestablishment were indistinguishable under our conditions (Figure 3, C and D). This observation suggests that chromatin modifications and Polycomb complex recruitment that were established during the initial spreading of *Xist* did not alter the kinetics of *Xist* spreading after cell division in a measurable manner.

We were able to follow one cell through an entire division cycle (Figure 4, A and B). In this cell we noted an intriguing biphasic behavior of the *Xist*-covered area. Measurement of the area of the *Xist* territory showed that a plateau was reached 1.5 h after the initial detection of *Xist* (Figure 4B). The area of the *Xist* cluster then remained stable for the next 3 h and increased again over the

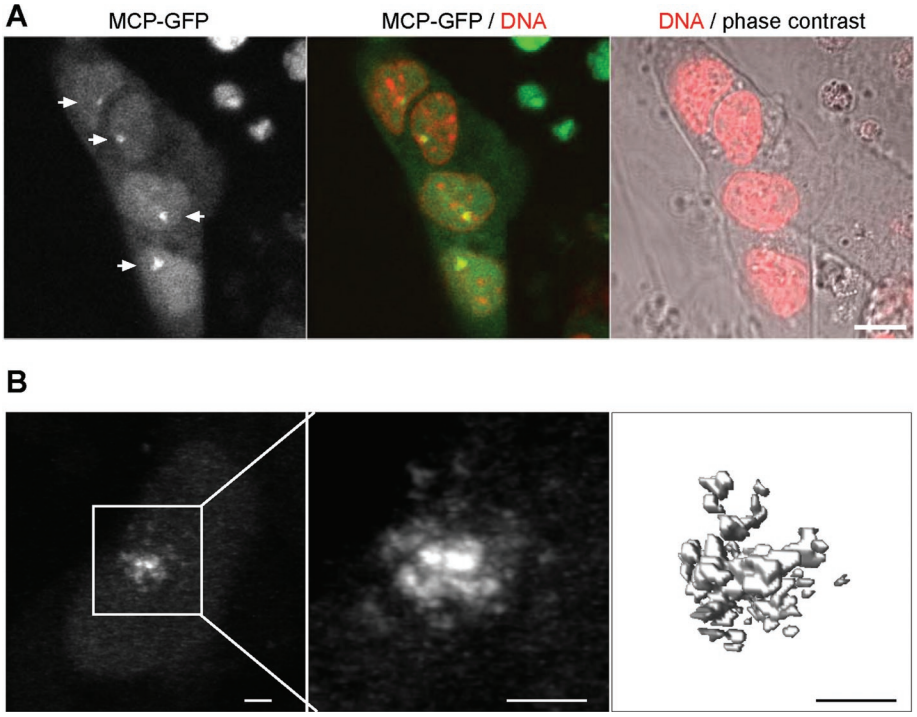

FIGURE 2: Imaging *Xist* in living cells. (A) Live image of an XMG ES cell colony 12 h after induction. Arrows indicate *Xist* clusters. DNA is stained with Hoechst 33342 (red) and overlaid on phase contrast. Scale bar, 10 μm. (B) High-resolution image of an *Xist* cluster in live XMG ES cells 12 h after induction. Projection of a confocal image stack of the nucleus, a higher magnification of the *Xist* cluster, and a 3D reconstruction are shown. Scale bars, 2 μm.

following ~2.5 h, when it reached a second plateau. We were able to measure this larger *Xist* cluster for 3 h before the cell entered mitosis and *Xist* was displaced. To test whether the increase in the *Xist* territory size between the two plateaus could be caused by the progression of the cell through S phase, we measured the area of the *Xist* cluster in image series of cells that had progressed through mitosis. Analysis of 10 individual cells showed that the *Xist* cluster size increased from 6.1 ± 1.1 μm^2 to 12.3 ± 2.5 μm^2 between the G1 and G2 phases of the cell cycle, respectively. To further investigate this observation, we measured the fluorescence intensity of the *Xist* cluster in fixed XMG ES cells. Nuclei were classified as either G1 or G2 based on the total DNA content as measured by DNA staining using Hoechst 33342 fluorescent dye. On average the *Xist* territory contained twice as much GFP fluorescence intensity in G2 than in G1 (Figure 4C). We further isolated G1 and G2 fractions of XMG ES cells by flow sorting. After staining DNA in living cells with Hoechst 33342 dye a clear G1 peak and a broader S/G2 area was observed, from which a G2/M area could be selected (Figure 4D). Analysis of *Xist* by quantitative real-time PCR showed that G2 cells contain three times the amount of *Xist* of G1 cells when normalized to total RNA (Figure 4D). This compares to a twofold increase in *Gapdh* mRNA. Taken together, our data show that between G1- and G2-phase cells the area of the *Xist* cluster and the amount of bound *Xist* increase, consistent with the idea that replication of chromosomal DNA increases the capacity of the chromosome to bind *Xist*.

Dynamics of *Xist* binding within the chromosome territory

To investigate the dynamics of *Xist* after the cluster had reached a plateau, we performed fluorescence recovery after photobleaching (FRAP) experiments (Cole *et al.*, 1996). First we investigated cells under continuous induction with Dox. We bleached chromosome-bound *Xist* by exposing an area overlapping the *Xist* cluster to high-intensity light. Under our conditions between 60 and 90% of the total fluorescence of the cluster was lost after bleaching. Time-lapse imaging after photobleaching showed that within 20–30 min fluorescence recovered to ~60–80% of the initial intensity throughout the territory and then appeared to remain stable (Figure 5A).

We next investigated *Xist* when new synthesis of *Xist* is inhibited by blocking transcription with actinomycin D (ActD). After blocking transcription, the *Xist* territory remained stable for more than 1 h (Figure 5C). When the *Xist* cluster was photobleached in the presence of ActD, fluorescence recovery of *Xist* was not observed (Figure 5B). This suggested that *Xist* dynamics required transcription. It was important to rule out any effects of ActD treatment. For this we stopped the production of *Xist* by washing out Dox from cells that had been induced overnight. We then carried out FRAP experiments on cells showing a stable *Xist* cluster 30 min after Dox depletion. Under these conditions no recovery of the *Xist* territory was observed, whereas in control cells that were cultured in the presence of Dox fluorescence recovered rapidly (Supplemental Figure S1, A and B). Taken together, these observations indicate that chromosome-bound *Xist* displays greater dynamics when transcription is not blocked.

To visualize the displacement of chromosome-bound *Xist* from the chromosome territory, we used inverse FRAP (iFRAP) experiments. We photobleached the unbound pool of MCP-GFP excluding the *Xist* cluster and measured the fluorescence of the *Xist* cluster over time (Figure 6A). We observed that the total fluorescence intensity of the *Xist* cluster decayed rapidly after iFRAP and reached a constant level after 10 min (Figure 6B). The decay of fluorescence intensity over time fitted well to a single-exponential model, indicating a first-order kinetics (Figure 6, C and D). Taken together, our observations suggest that *Xist* reversibly attaches to the chromosome, consistent with a dynamic turnover of *Xist* within the established cluster.

DISCUSSION

Here we describe a system for imaging *Xist* RNA in living cells. Although clearly the system does not reflect endogenous X inactivation, we can show that gene repression and histone modifications are recapitulated by transgenic *Xist*-MS2 in an autosomal context. We suggest that our system might be useful for initial observations of *Xist* spreading, given that there has been little progress with attempts for imaging endogenous *Xist*. Several considerations make our transgenic system preferable. First, analysis of endogenous X inactivation requires imaging in difficult conditions such as the early mouse embryo or differentiating ES cell cultures by which cell types and physiological parameters are changing. We can image in mouse ES cells, which are a highly homogeneous culture system. Second, using inducible expression of *Xist* provides enhanced experimental control over *Xist* transcription, which enabled us to perform crucial control experiments.

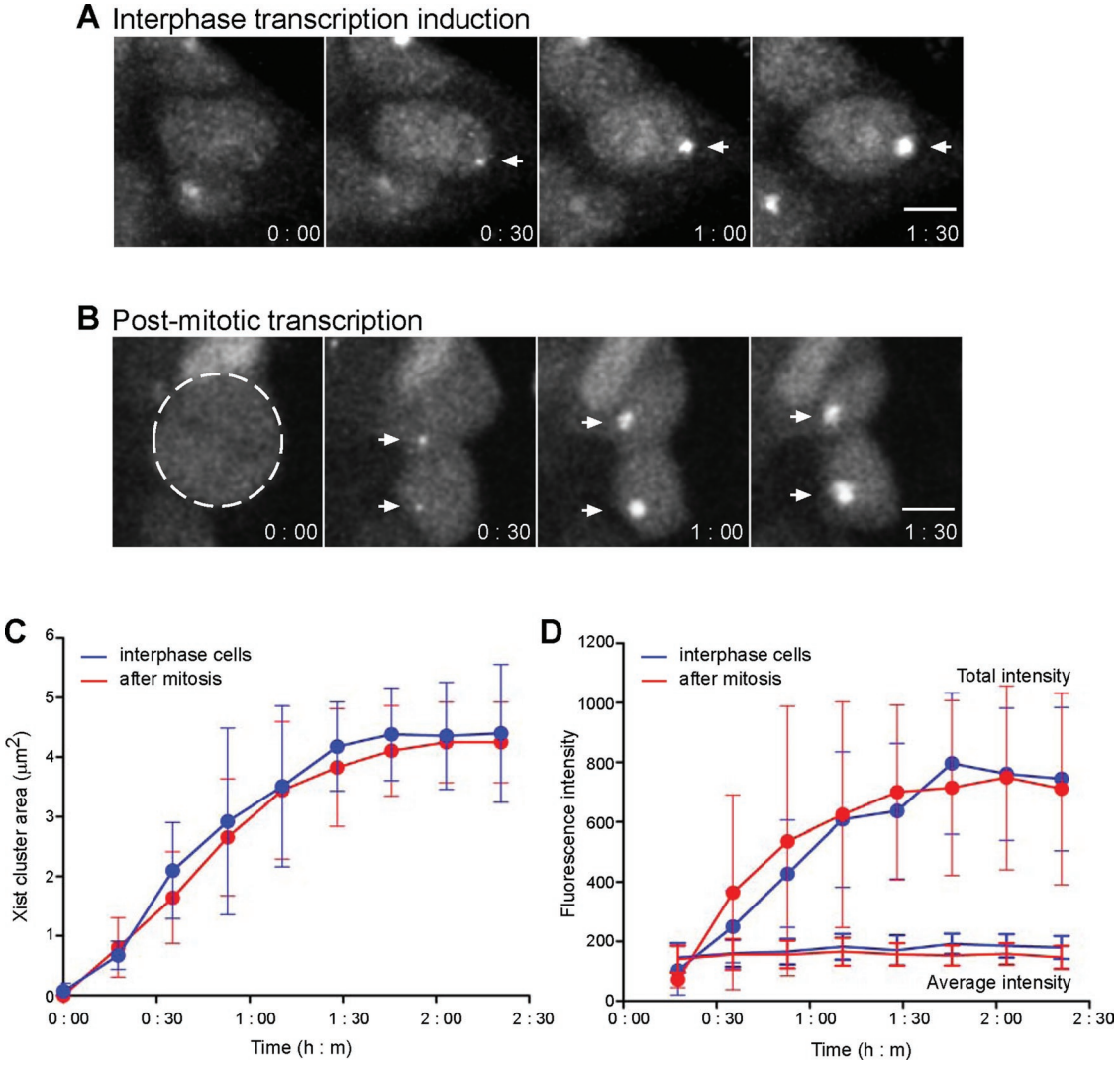

FIGURE 3: De novo establishment of *Xist* binding after first induction or mitosis. (A) Confocal images of *Xist* accumulation at selected time points (hours:minutes) after the addition of Dox (0:00 is the last image before an *Xist* focus was first detected). Arrows indicate the *Xist* territory. Scale bar, 5 μm. (B) XMG cells induced with Dox were followed through mitosis (time set to 0:00 at metaphase). Confocal images of *Xist* accumulation at selected time points (hours:minutes) after mitosis are shown. Arrows indicate the *Xist* territory. The mitotic cell is outlined with a dotted line. Scale bar, 5 μm. (C) The kinetics of *Xist* accumulation after initial induction in interphase (blue) and after mitosis (red). The area of the *Xist* clusters was measured, and the average of 10 cells each is plotted over time. Error bars indicate the SD. (D) The total fluorescence intensity (filled circles) and average fluorescence intensity of the *Xist* cluster is plotted over time as in C.

Using this system, we have confirmed previous studies of *Xist* localization in living cells and made several new observations. Consistent with earlier work, we show that *Xist* spreads from a single spot over the chromosome until it is lost at mitosis. We extend previous studies by showing that spreading from a single site leads to saturation of the chromosome with *Xist*. Our study also gives a first idea of the time required to cover a chromosome with *Xist*. We determined that *Xist* accumulated within 1.5 h, which is a significant amount of time at the initiation of X inactivation. We further find that the amount of *Xist* approximately doubles between G1 and G2 phases of the cell cycle, indicating that the binding capacity is proportional to the amount of chromosomal DNA. This is compatible with the idea that distinct DNA sequences such as LINE elements or chromatin regions act as *Xist* attachment sites and their duplication during replication leads to an increase in *Xist* binding. One surprising finding is that the spreading of *Xist* after initial induction and reestablishment of the *Xist* cluster after mitosis follow similar kinetics. This observation suggests that chromatin modifications do not have a measurable influence on *Xist* spreading. One limitation of this result is that we performed our studies in mouse ES cells, where X inactivation is reversible. Therefore our data do not rule out that changes in *Xist* spreading might be induced after entry into differentiation.

Our live-imaging system afforded us the opportunity to analyze the dynamics of chromosome-bound *Xist*. Measurements by FRAP and iFRAP indicate that *Xist* is dynamically bound and is replaced by newly synthesized *Xist* within the established cluster. This analysis critically depends on the stability of the *Xist* MS2 MCP-GFP interaction. Exchange of MCP-GFP on the *Xist*-MS2 RNA in the time scale of our measurements could seriously undermine our

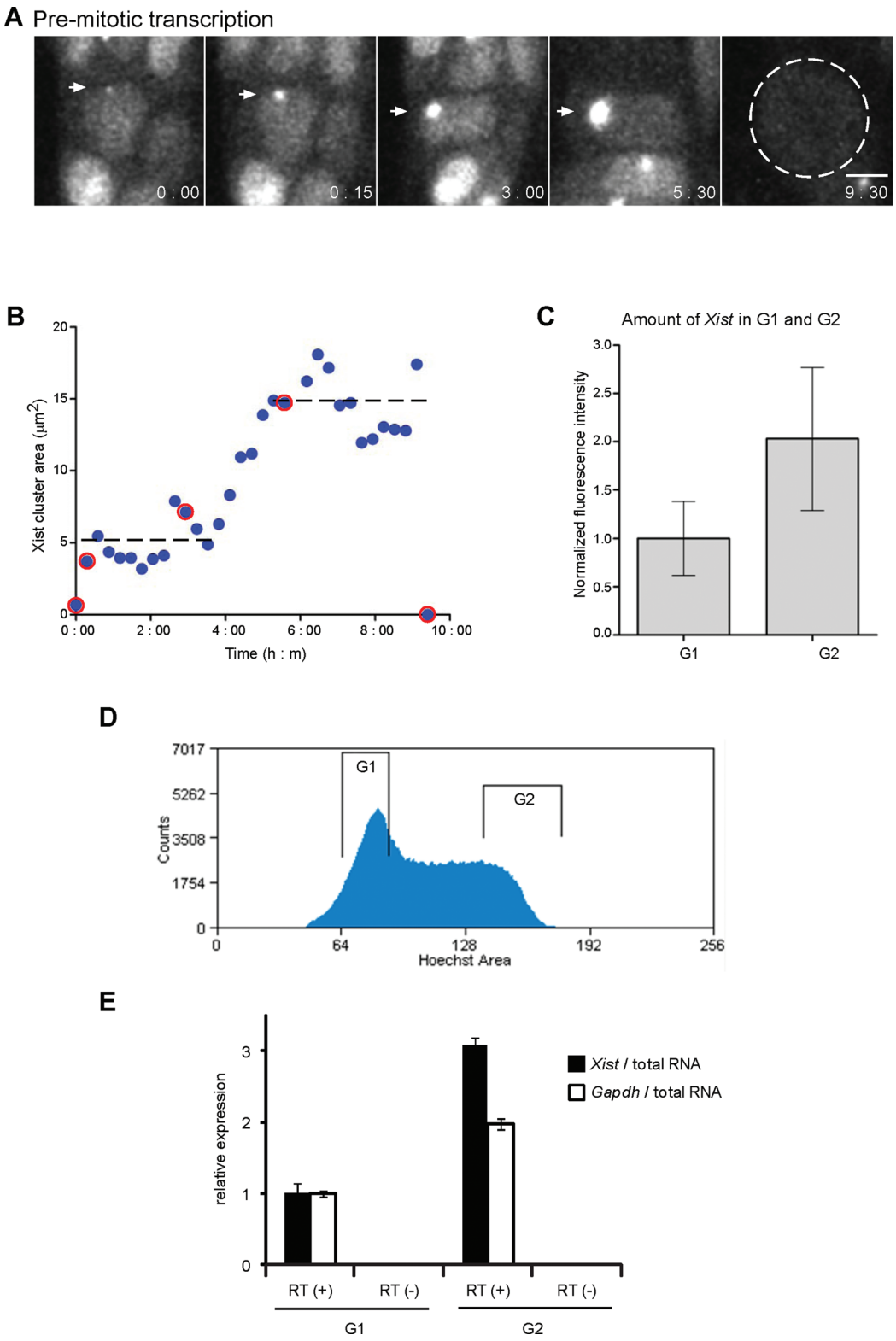

FIGURE 4: Amount of chromosome-bound *Xist* increases during S phase. (A) Premitotic accumulation of *Xist* at selected time points (hours:minutes) after the addition of Dox (0:00 is the image at the first appearance of the *Xist* focus). Scale bar, 5 μm. (B) The area of the *Xist* cluster in the premitotic cell, shown in A, measured over time. Red open circles represent the data points from the images in A. Dotted line represents the average size of the *Xist* cluster in the first and second plateaus of the data curve. (C) Statistics of the total fluorescence intensity of the *Xist* clusters of XMG ES cells in G1 and G2. G1 and G2 cells were defined by DNA content measured by Hoechst 33342 staining. The average of 15 cells is plotted, with error bars indicating the SD. (D) FACS profile of XMG cells stained with Hoechst 33342 with regions of G1 and G2 fractions indicated. (E) Quantitative real-time PCR analysis of *Xist* and *Gapdh* expression in G1 and G2 phases. Expression is expressed relative to total RNA, and the G1-phase expression levels were set to 1. Error bars represent SD (n = 3).

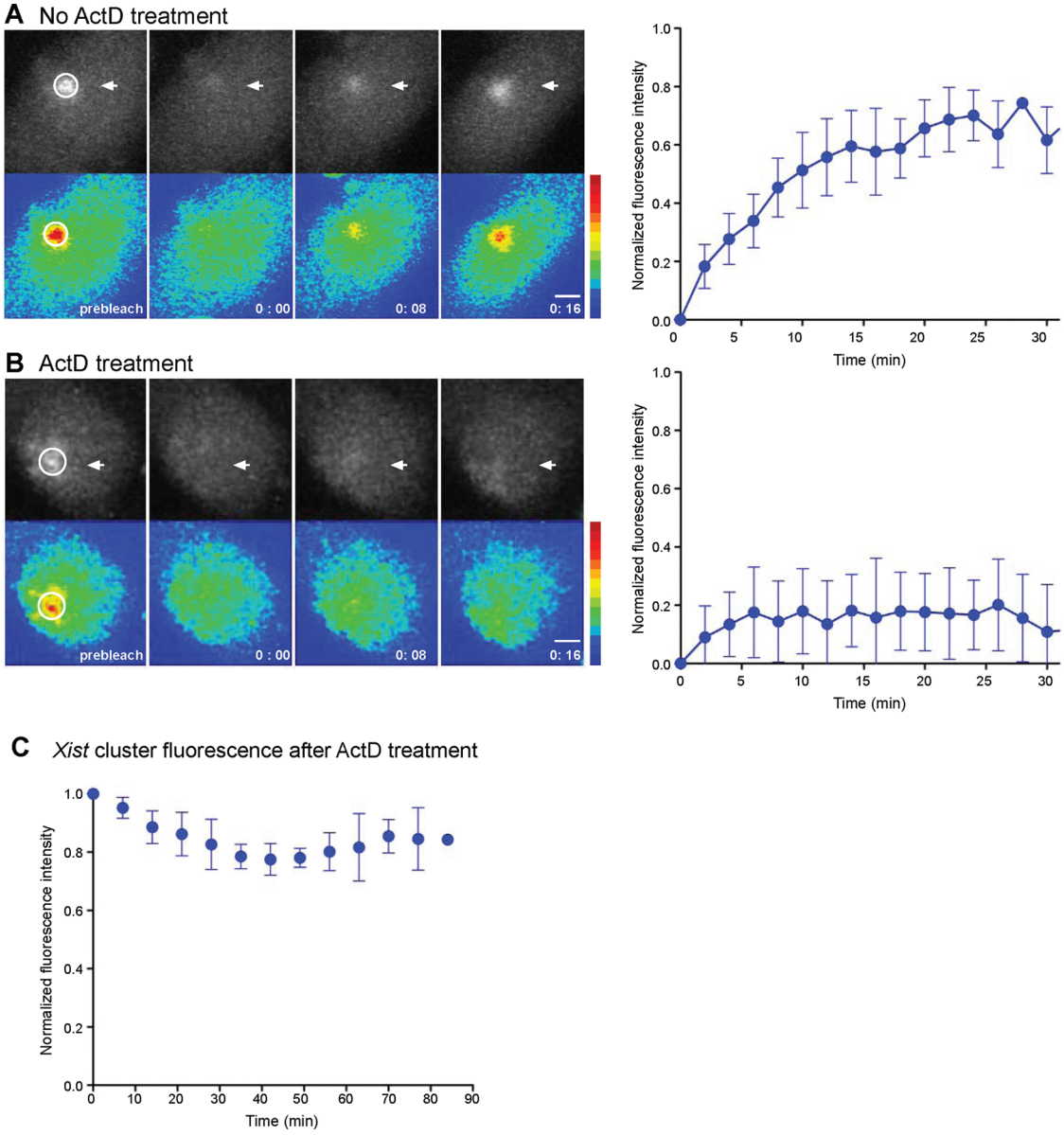

FIGURE 5: Turnover of *Xist* RNA within the chromosome territory in steady state. FRAP analysis of *Xist* dynamics in interphase XMG ES cells without (A) and with (B) ActD. A confocal image sequence (hours:minutes) is shown (left) in gray scale (top) and in pseudocolor (bottom). XMG ES cells were induced for *Xist* expression for 4 h prior to FRAP analysis, and photobleaching of the entire *Xist* cluster (circle) was carried out 10 min after the addition of 10 μg/ml ActD. Scale bar, 2 μm. The normalized signal intensity of the *Xist* cluster after photobleaching is plotted over time (right; n = 9). Error bars indicate the SD. (C) *Xist* remains stable for at least 80 min after the addition of ActD. *Xist* cluster intensity in living XMG ES cells normalized to nuclear background intensity is plotted against time. Error bars represent the SD from six cells.

analysis. In vitro measurements estimated that the complex of the C-variant MS2 RNA motif and the RNA-binding protein dissociates with a half-life of 408 min, or more than 6 h, which would certainly be long enough for measuring in the 30-min interval of our experiment (Lowary and Uhlenbeck, 1987). However, this might be changed in the in vivo context of our experiment. A recent study used a similar system to measure the dynamics of *gurken* mRNA in *Drosophila* egg chambers with half-lives in the order of minutes (Jaramillo *et al.*, 2008). In our setup quasi-static binding of *Xist* when transcription is blocked (Clemson *et al.*, 1996; Wutz and Jaenisch, 2000; Seidl *et al.*, 2006; Sun *et al.*, 2006) can serve as an additional control by separating the two components of fluorescence recovery. When *Xist* transcription is blocked, fluorescence recovery can only come from the exchange of bleached for green MCP-GFP molecules on the bound *Xist*-MS2. We did not observe measurable recovery of fluorescence within 30 min after FRAP. Results after washout of Dox or actinomycin D transcription inhibition confirm a long-lived interaction between the MCP-GFP protein and the MS2-tagged *Xist*-MS2 in our system. We therefore believe that our observations on the dynamic binding of *Xist* might be mechanistically relevant.

To obtain an estimate for the half-life of bound *Xist* in our system we used the loss of fluorescence in our iFRAP experiments. These

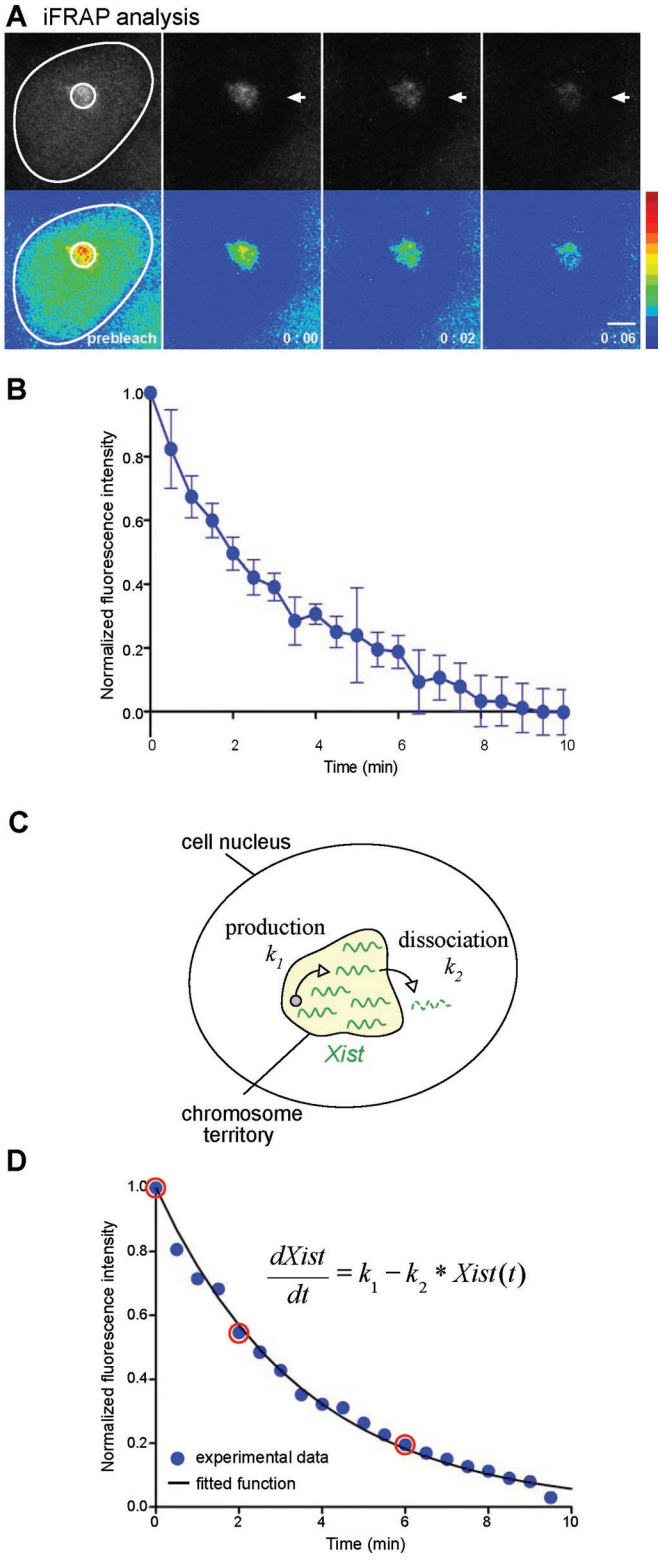

FIGURE 6: Displacement of chromosome-bound *Xist*. (A) iFRAP analysis of *Xist* turnover in XMG ES cells. A confocal image series is shown in gray scale (top) and in pseudocolor (bottom). The nuclear pool of MCP-GFP outside the *Xist* territory was photobleached (white outline). Scale bar, 2 μm. (B) The normalized signal intensity of the iFRAP experiment of the *Xist* cluster is plotted over time (n = 4). Error bars represent SD. (C) *Xist* turnover is characterized by its production with rate k_1 from the site of transcription and loss due to dissociation off the chromosome with the dissociation constant k_2. After dissociation *Xist* is degraded. In steady state the *Xist* cluster is stable, and production and dissociation balance. (D) The normalized signal intensity of the single experiment shown in A is plotted over time. Red open circles indicate data points of the images in A. The data points were fitted to a kinetic model of *Xist* transcription and dissociation (black line).

data fitted well to a single-exponential model where the steady-state *Xist* concentration in the cluster results from the balance of transcription of new *Xist* and dissociation of old bound *Xist* from the territory (Figure 5C). From this a rate of dissociation for *Xist* of 0.006 ± 0.0007 s^{-1} was obtained. This corresponds to a residence time of *Xist* within the chromosome territory on the order of 3 min (Figure 6, C and D). How this dynamics compares to that of the endogenous *Xist* is unclear. It has been reported that *Xist* is continuously transcribed even in differentiated cells (Clemson *et al.*, 1996). Therefore turnover of *Xist* is expected to be associated with the Xi. Our measurements might provide an upper bound for *Xist* turnover. Taking into account that a high rate of *Xist* production from the seven copies of *Xist* in XMG ES cells almost certainly leads to overexpression of *Xist* to some degree, it is likely that *Xist* is less dynamic during normal X inactivation. Furthermore, it is unknown whether the addition of the GFP protein molecules to *Xist* could have influenced its behavior. However, we note that in our transgenic system several features of X inactivation are recapitulated under conditions of highly dynamic *Xist* turnover.

Our iFRAP measurements consistently give shorter recovery times than our FRAP measurements. This might be explained by the need to bind MCP-GFP molecules to newly transcribed *Xist*-MS2, whereas the iFRAP experiment measures the dissociation of already MCP-GFP–labeled *Xist*. This suggests that a significant amount of time is required for MCP-GFP binding, which could involve folding of the MS2 RNA motif and diffusion of MCP-GFP molecules within the chromosome territory. Although dynamics measurements by fluorescence correlation spectroscopy (FCS) indicate that MCP-GFP diffusion is not limiting our kinetic measurements (Supplemental Figure S2), local effects within the chromosome territory could lead to diffusion kinetics that differ substantially from the overall measurements in the nucleus. The idea of local effects in MCP-GFP diffusion and binding could eventually explain the fact that we rarely observed more than 80% recovery of the *Xist* cluster after FRAP. Local binding of bleached MCP-GFP to newly transcribed *Xist* is a likely explanation for this observation. Formally the difference between the kinetics measured in our FRAP and iFRAP experiments could also be the result of different amounts of light-induced changes or damage of chromatin during photobleaching. However, we consider this unlikely, as the low fluorescence signal of the *Xist* cluster and the nuclear MCP-GFP were easily photobleached with relative low light intensity. Under these conditions nuclear damage can be ruled out, making it unlikely that *Xist* dynamics was affected by photobleaching.

Less than complete recovery of fluorescence also opens up the possibility that a fraction of up to 20% of *Xist* is stably bound. We do not favor this idea, as a fraction of 20% of *Xist* would have been easily detected in our iFRAP experiments, where we find no indication. Notably, over 90% of *Xist* within the cluster becomes stably bound when transcription is arrested, showing that the switch to stable binding is not caused by different populations of *Xist*.

In our study we observe that the kinetics of *Xist* within an established cluster is twice as fast as the initial establishment of the *Xist* cluster after mitosis or induction of expression. This suggests that

once the chromosome is covered with *Xist*, newly synthesized *Xist* can bind more rapidly than on a chromosome that is not decorated with *Xist*. We think this might reflect changes in the organization of chromatin that are induced by *Xist* binding. Chromatin modifications might play a lesser role for *Xist* binding, as we have observed similar kinetics of *Xist* accumulation after initial induction and after mitosis when chromatin modifications are inherited from the previous cell cycle.

The kinetics of *Xist* turnover with and without transcription differ by nearly two orders of magnitude, with half-lives of 3 min and 4–6 h, respectively. The very long half-life of *Xist* after transcription block indicates a very stable attachment and a corresponding high binding energy. An interesting question is then how this substantial energy barrier is overcome when newly synthesized *Xist* displaces chromatin bound *Xist*. We speculate that the binding energy could be overcome if *Xist* were displaced by a stepwise takeover of individual interactions along the RNA. Alternatively, *Xist* binding could be regulated, consistent with a report that Aurora B kinase has a role in the displacement of *Xist* during mitosis (Hall *et al.*, 2009).

Observations from visualization of *Xist* in living cells have uncovered a dynamic behavior that might be important for understanding the mechanism of *Xist* function. Further studies will be needed to confirm our results during normal X inactivation. *Xist* has exclusively evolved in placental mammals (Duret *et al.*, 2006; Elisaphenko *et al.*, 2008) and presents a model for noncoding RNA function in chromatin compartmentalization (Heard and Bickmore, 2007). In light of recent discoveries of large sets of long noncoding RNAs (Rinn *et al.*, 2007; Guttman *et al.*, 2009; Khalil *et al.*, 2009; Ponting *et al.*, 2009), live imaging might also be a useful approach for studying the role and dynamics of other noncoding transcripts in mammalian cells. We are confident that dynamics will prove a vital aspect of noncoding RNA function and our live-imaging system might introduce a new tool.

MATERIALS AND METHODS

Vector construction

ptetOP-MS2 was generated by directional cloning of the *Bam*HI (blunt)-*Sph*I fragment of 24x MS2 (Fusco *et al.*, 2003) into the *Eco*NI (blunt)-*Sph*I site of ptetOP H/X vector (Wutz and Jaenisch, 2000). The *Cla*I-*Pvu*I fragment was then inserted into ptetOP-*Xist*-PA vector (Wutz and Jaenisch, 2000) and digested with *Cla*I-*Pvu*I, giving ptetOP-*Xist*-MS2-PA. For pCAG-MCP-GFPnls the *Cla*I-digested nlsMCP(dIFG)-GFP fragment from plasmid hsp83-MCP(dIFG)-GFP (a gift from P. Becker) was inserted into the *Eco*RI-digested pCAG vector (Niwa *et al.*, 1991).

Cell culture and generation of cell lines

The XMG cell line was generated by a two-step random integration strategy into J1 ES cells, which contained nlsrtTA targeted in the ROSA26 locus (Wutz and Jaenisch, 2000). First, 100 μg of ptetOP-*Xist*-MS2-PA and 10 μg pf pPGKpuro plasmid, both linearized, were coelectroporated into J1 ES cells to create the XM cell line. Puromycin (2 μg/ml)–resistant colonies were individually selected and screened for expression by *Xist*/MS2 RNA FISH after 24 h of induction on Roboz slides (CellPoint Scientific, Gaithersburg, MD). Second, 100 μg of pCAG-MCP-GFP-nls with 10 μg of pPGKhygro, both linearized, were cointegrated into the XM cell line. Stable expressing clones were identified after selection with hygromycin B (130 μg/ml) for 8 d. Positive clones were verified under the fluorescence microscope after 24-h induction on Roboz slides and confirmed by flow cytometry (FACsort; BD Biosciences, Franklin Lake, NJ). After further subcloning, a cell line was isolated that allowed imaging of *Xist* in the majority of cells.

RNA and DNA FISH analysis

ES cells were attached to poly-L-lysine–coated slides (Sigma-Aldrich, St. Louis, MO) by using a Shandon Cytospin 3 centrifuge (Thermo Fisher Scientific, Waltham, MA). RNA FISH was performed as described (Wutz and Jaenisch, 2000). Briefly, cells were permeabilized with CSK buffer/0.5% Triton X-100 for 2 min, fixed with 4% paraformaldehyde (PFA) in phosphate-buffered saline (PBS) for 10 min, and dehydrated progressively in ethanol. Hybridizations were performed overnight at 37°C in a dark and humid chamber, followed by washing three times in 50% formamide/2× saline sodium citrate (SSC), three times in 2× SSC for 5 min each at 39°C, and once in 1× SSC for 10 min at room temperature. Slides were counterstained with 4′,6-diamidino-2-phenylindole (DAPI), mounted with coverslips, and analyzed. The coordinates of the cells on the slides were recorded on the microscope. Following RNase treatment (100 μg/ml) at 37°C for 30 min, cells were denatured in 70% formamide/2× SSC at 80°C for 10 min and rinsed in 2× SSC prior to overnight hybridization for sequential DNA FISH. For DNA FISH analysis, cells were fixed with methanol-acetic acid (3:1), dropped onto poly-L-lysine–coated slides, denatured at 80°C for 5 min, and subsequently hybridized.

Probes were labeled using random priming (PrimeIt; Stratagene, Santa Clara, CA) with cy5-dCTP or cy3-dCTP (Amersham, GE Healthcare, Piscataway, NJ). *Xist* was excised from ptetOP-*Xist*-PA (Wutz and Jaenisch, 2000) and MS2 from 24x MS2 (Fusco *et al.*, 2003).

Immunofluorescence and protein analysis

Immunofluorescence combined with RNA FISH was performed as described (Chaumeil *et al.*, 2006). For GFP immunofluorescence, cells were fixed for 10 min at room temperature in 4% PFA in PBS, permeabilized for 5 min at room temperature (RT) in 0.1% Na citrate/0.1% Triton X-100, and blocked for 60 min at RT in PBS containing 5% (wt/vol) bovine serum albumin, 0.1% Tween-20. GFP was detected using a mixture of mouse monoclonal clone 7.1 and 13.1 anti-GFP antibody at 1:500 (#11814460001; Roche, Indianapolis, IN) followed by Alexa A-11034 Fluor 488 goat anti–mouse immunoglobulin G (IgG) (H+L) at 1:500 (Molecular Probes; Invitrogen, Carlsbad, CA). For combined H2AK119ub1/H3K27me3 immunofluorescence, cells were preextracted in 100 mM NaCl, 300 mM sucrose, 3 mM $MgCl_2$, 10 mM 1,4-piperazinediethanesulfonic acid, pH 6.8, and 0.5% Triton for 2 min at room temperature. Histone modification H3K27me3 was detected using α-H3K27me3 at 1:1000 (#6523) (Schoeftner *et al.*, 2006), followed by Alexa Fluor 488 goat anti–rabbit IgG (H+L) at 1:500 (Molecular Probes) staining. H2AK119ub1 primary antibody α-ubiquityl-histone H2A at 1:50 (clone E6C5; #05–678; Upstate Biotechnology, Waltham, MA) followed by secondary antibody Alexa Fluor 568 goat anti–mouse IgG (H+L) at 1:500 (Molecular Probes). After immunofluorescence, cells were fixed in 4% PFA in PBS for 10 min at room temperature, dehydrated, hybridized, and washed as described for RNA FISH.

For Western analysis ES cells were grown for 2 d without feeders. Nuclear extracts were prepared and analyzed by SDS–PAGE as described (Schoeftner *et al.*, 2006). GFP was detected with a mixture of mouse monoclonal clone 7.1 and 13.1 anti-GFP antibody at 1:200 (#11814460001; Roche) and a horseradish peroxidase–conjugated AffiniPure goat anti–mouse IgG (H+L), 1:5000 (Jackson ImmunoResearch Laboratories, West Grove, PA), secondary antibody. Chemiluminescence reagent (ECL; Amersham) and imaging film (Biomax; Eastman-Kodak, Rochester, NY) were used for detection.

Live cell microscopy and data analysis

Confocal images were acquired on a Zeiss LSM510 microscope. For live-cell observation, cells were grown in Lab-Tek chamber coverglasses (Nunc, Thermo Fisher Scientific) overnight in the presence of feeders. Dox (1 µg/ml) was added to the cells 4 h before imaging. Prior to imaging, the medium was changed to prewarmed CO_2-independent medium without phenol red (Invitrogen) containing 1 µg/ml Dox, unless otherwise stated, and was sealed with silicon grease. Where indicated, DNA was stained in live cells by 0.2 µg/ml Hoechst 33342. For ActD experiments, 20 µg/ml ActD (Sigma-Aldrich) was added as a 2× solution to imaging medium for 10 min before the experiment. Single confocal sections or three-dimensional stacks of live cells were captured automatically (Rabut and Ellenberg, 2004) using a Zeiss LSM510 confocal microscope with a 63× oil immersion objective (Gerlich *et al.*, 2006). For FRAP experiments three iterations of photobleaching at 100- to 500-fold the acquisition laser intensity with 100% transmission of 488-nm laser on either the entire *Xist* cluster or half the *Xist* cluster or the nucleoplasm were used. The first postbleach frame was acquired immediately after photobleaching. A time series of typically six confocal z sections (3-µm pinhole with 2-µm z-intervals) was recorded with 2-min intervals for a total of 30 min for untreated cells and 60 min for ActD-treated cells.

Images were adjusted by the brightness and contrast and filtered using a low-pass filter implemented in the LSM510 software and then assembled in ImageJ and cropped. For 3D reconstruction, Imaris (Bitplane, South Windsor, CT) was used. Quantification was carried out using ImageJ. Fluorescence recovery in photobleaching experiments was measured in fixed-size user-defined cellular regions in 3D projection of the z-stacks at all time points. To measure the area of *Xist* territories during cell cycle, images were thresholded with the mean background value plus two times the SD of the background. FRAP experiments, which show a signal-to-noise ratio of >2 and *Xist* clusters ~2 µm in diameter, were quantified and were normalized to the initial fluorescence-intensity distribution and to total fluorescence, thereby correcting for movements in z-plane and for fluorescence decay due to postbleach acquisition (Rabut and Ellenberg, 2004). FRAP and iFRAP experiments were normalized to the initial *Xist* cluster intensity, and the normalized intensity value for the *Xist* cluster, I_{norm}, was measured for each time point:

$$I_{norm} = \left[\left(\frac{I_{Xist}(t) - I_{BG}(t)}{I_{Nu}(t) - I_{BG}(t)}\right) - \left(\frac{I_{Xist}(t = postbl) - I_{BG}(t = postbl)}{I_{Nu}(t = postbl) - I_{BG}(t = postbl)}\right)\right] \div \left[\left(\frac{I_{Xist}(t = prebl) - I_{BG}(t = prebl)}{I_{Nu}(t = prebl) - I_{BG}(t = prebl)}\right) - \left(\frac{I_{Xist}(t = postbl) - I_{BG}(t = postbl)}{I_{Nu}(t = postbl) - I_{BG}(t = postbl)}\right)\right] \quad (1)$$

where I_{Xist} and I_{Nu} are the *Xist* cluster and total nuclear background corrected intensities, respectively, prebl is prebleached, and postbl is postbleached. I_{BG} is the background intensity outside the nucleus.

Kinetic modeling: *Xist* is produced by transcription at a constant rate (k_1); it then binds to chromatin, and its association is characterized by a dissociation constant (k_2). At steady state, production and dissociation are balanced and define the number of *Xist* bound to the chromosome, $Xist^{st} = k_1/k_2$. *Xist* dynamics can be described with a first-order kinetics:

$$\frac{dXist}{dt} = k_2(Xist^{st} - Xist) \quad (2)$$

This equation was used to fit FRAP/iFRAP experiments, in which the MCP-GFP shuttling can be neglected.

For experiments involving washing out Dox for turning *Xist* transcription off, cells were grown on ibiTreat µ-Slide eight-well slides (ibidi, Martinsried, Germany) coated with gelatin (Figure S1). Cells were cultured overnight in the presence of 1 µg/ml Dox. Before imaging, Dox was washed out by five times replacing the medium with fresh prewarmed medium without Dox. After 30 min, *Xist* transcription became negligible. These ibidi slides provided superior adhesion for ES cells, allowing for repeated washes without cell displacement. Best imaging conditions were found using a 63× oil immersion objective on a Leica SP5 confocal microscope with inverted DMI6000 stands fitted with environmental cube housings for live-cell imaging.

Fluorescence correlation spectroscopy

Fluorescence correlation spectroscopy (FCS) was performed at room temperature using a Zeiss LSM FCS Confocor2 with a 40× water immersion objective (numerical aperture, 1.2) It records fluorescence intensity fluctuations, which were analyzed using the autocorrelation function of the intensity signal, which can be adjusted with the anomalous diffusion model (Bancaud *et al.*, 2009). This technique enabled us to measure the MCP-GFP nucleoplasmic diffusion coefficient and concentration based on anomalous diffusion fitting (Haustein and Schwille, 2007):

$$ACF(t) = \frac{1}{\langle N \rangle} \times \frac{1}{\left\{1 + \left(\frac{t}{t_D}\right)^{2/\beta}\right\} \times \left\{1 + \frac{1}{S^2}\left(\frac{t}{t_D}\right)^{2/\beta}\right\}^{0.5}} \quad (3)$$

where $\langle N \rangle$ is the mean number of tracers in the confocal volume, τ_D is the mean residence time in the confocal volume, S^2 is the structure parameter, which is defined by the confocal volume equatorial-to-axial dimension ratio, and β is the anomaly parameter. According to Zeiss specifications, the confocal volume axial and equatorial dimensions are typically 0.3 and 1.5 µm, respectively, so S was set to 5. The fit using (3) enables us to measure MCP-GFP nucleoplasmic residence time (Supplemental Figure 2) and the nucleoplasmic concentration of MCP-GFP, given the confocal volume dimension. On the basis of combining FCS with confocal imaging, the onset of MCP-GFP concentration in the *Xist* territory was subsequently extracted, providing an estimate for the number of MCP-GFP bound to *Xist*. Assuming that 33 MCP-GFP bind to one *Xist* RNA (Fusco *et al.*, 2003), we could calculate the steady-state number of *Xist* molecules.

Expression analysis of G1- and G2-phase cells

XMG ES cells were cultured overnight in the presence of 1 µg/ml Dox. Approximately 5×10^6 cells were harvested and incubated with Hoechst 33342 dye diluted 1:100 in medium containing 1 µg/ml Dox for 30 min at 37°C. Sorting of the cells was performed on a Dako MoFlo cell sorter (Beckman Coulter, Brea, CA). Total RNA was isolated from equal numbers of G1- and G2-phase cells using TRIzol (Invitrogen). RNA concentration was determined on a NanoDrop spectrophotometer.

Quantitative real-time PCR of gene expression was performed using the Fast SYBR Green Master Mix and the StepOnePlus Real-Time PCR System (Applied Biosystems, Foster City, CA). Sequences for primers for detection of *Xist* were TCATCACAACAGCAGTTCTC and CAGGAGCACAAAACAGACTC. *Gapdh* was detected using the previously published primer set Gapd F and Gapd R2 (Sado *et al.*, 2005).

ACKNOWLEDGMENTS

We thank L. Klein and M. Busslinger for critical discussion of the manuscript and P. Becker for providing the hsp83-MCP(dIFG)-GFP plasmid. J.E. acknowledges support from the European Molecular Biology Laboratory and the German National Research Council (DFG EL 246/2-2). A.B. was funded through a Federation of European Biochemical Societies postdoctoral fellowship. A.W. is supported by a Wellcome Trust Senior Research Fellowship (Grant Reference 087530/Z/08/A). This work was supported by the Research Institute of Molecular Pathology and by a grant from the Austrian Science Fund (Grant Reference SFB17 FWF).

REFERENCES

Agrelo R *et al.* (2009). SATB1 defines the developmental context for gene silencing by *Xist* in lymphoma and embryonic cells. Dev Cell 16, 507–516.

Bancaud A, Huet S, Daigle N, Mozziconacci J, Beaudouin J, Ellenberg J (2009). Molecular crowding affects diffusion and binding of nuclear proteins in heterochromatin and reveals the fractal organization of chromatin. EMBO J 28, 3785–3798.

Barakat TS, Jonkers I, Monkhorst K, Gribnau J (2010). X-changing information on X inactivation. Exp Cell Res 316, 679–687.

Beard C, Li E, Jaenisch R (1995). Loss of methylation activates *Xist* in somatic but not in embryonic cells. Genes Dev 9, 2325–2334.

Bertrand E, Chartrand P, Schaefer M, Shenoy SM, Singer RH, Long RM (1998). Localization of ASH1 mRNA particles in living yeast. Mol Cell 2, 437–445.

Blewitt ME *et al.* (2008). SmcHD1, containing a structural-maintenance-of-chromosomes hinge domain, has a critical role in X inactivation. Nat Genet 40, 663–669.

Borsani G *et al.* (1991). Characterization of a murine gene expressed from the inactive X chromosome. Nature 351, 325–329.

Brockdorff N, Ashworth A, Kay GF, Cooper P, Smith S, McCabe VM, Norris DP, Penny GD, Patel D, Rastan S (1991). Conservation of position and exclusive expression of mouse *Xist* from the inactive X chromosome. Nature 351, 329–331.

Brown CJ, Ballabio A, Rupert JL, Lafreniere RG, Grompe M, Tonlorenzi R, Willard HF (1991a). A gene from the region of the human X inactivation centre is expressed exclusively from the inactive X chromosome. Nature 349, 38–44.

Brown CJ, Lafreniere RG, Powers VE, Sebastio G, Ballabio A, Pettigrew AL, Ledbetter DH, Levy E, Craig IW, Willard HF (1991b). Localization of the X inactivation centre on the human X chromosome in Xq13. Nature 349, 82–84.

Chaumeil J, Le Baccon P, Wutz A, Heard E (2006). A novel role for *Xist* RNA in the formation of a repressive nuclear compartment into which genes are recruited when silenced. Genes Dev 20, 2223–2237.

Chaumeil J, Okamoto I, Guggiari M, Heard E (2002). Integrated kinetics of X chromosome inactivation in differentiating embryonic stem cells. Cytogenet Genome Res 99, 75–84.

Chow JC, Hall LL, Baldry SE, Thorogood NP, Lawrence JB, Brown CJ (2007). Inducible *XIST*-dependent X-chromosome inactivation in human somatic cells is reversible. Proc Natl Acad Sci USA 104, 10104–10109.

Clemson CM, Hall LL, Byron M, McNeil J, Lawrence JB (2006). The X chromosome is organized into a gene-rich outer rim and an internal core containing silenced nongenic sequences. Proc Natl Acad Sci USA 103, 7688–7693.

Clemson CM, McNeil JA, Willard HF, Lawrence JB (1996). *XIST* RNA paints the inactive X chromosome at interphase: evidence for a novel RNA involved in nuclear/chromosome structure. J Cell Biol 132, 259–275.

Cole NB, Smith CL, Sciaky N, Terasaki M, Edidin M, Lippincott-Schwartz J (1996). Diffusional mobility of Golgi proteins in membranes of living cells. Science 273, 797–801.

Duret L, Chureau C, Samain S, Weissenbach J, Avner P (2006). The *Xist* RNA gene evolved in eutherians by pseudogenization of a protein-coding gene. Science 312, 1653–1655.

Elisaphenko EA, Kolesnikov NN, Shevchenko AI, Rogozin IB, Nesterova TB, Brockdorff N, Zakian SM (2008). A dual origin of the *Xist* gene from a protein-coding gene and a set of transposable elements. PLoS One 3, e2521.

Fackelmayer FO (2005). A stable proteinaceous structure in the territory of inactive X chromosomes. J Biol Chem 280, 1720–1723.

Fusco D, Accornero N, Lavoie B, Shenoy SM, Blanchard JM, Singer RH, Bertrand E (2003). Single mRNA molecules demonstrate probabilistic movement in living mammalian cells. Curr Biol 13, 161–167.

Fusco D, Bertrand E, Singer RH (2004). Imaging of single mRNAs in the cytoplasm of living cells. Prog Mol Subcell Biol 35, 135–150.

Gerlich D, Koch B, Dupeux F, Peters JM, Ellenberg J (2006). Live-cell imaging reveals a stable cohesin-chromatin interaction after but not before DNA replication. Curr Biol 16, 1571–1578.

Guttman M *et al.* (2009). Chromatin signature reveals over a thousand highly conserved large non-coding RNAs in mammals. Nature 458, 223–227.

Hall LL, Byron M, Pageau G, Lawrence JB (2009). AURKB-mediated effects on chromatin regulate binding versus release of *XIST* RNA to the inactive chromosome. J Cell Biol 186, 491–507.

Hall LL, Byron M, Sakai K, Carrel L, Willard HF, Lawrence JB (2002). An ectopic human *XIST* gene can induce chromosome inactivation in postdifferentiation human HT-1080 cells. Proc Natl Acad Sci USA 99, 8677–8682.

Hasegawa Y, Brockdorff N, Kawano S, Tsutui K, Tsutui K, Nakagawa S (2010). The matrix protein hnRNP U is required for chromosomal localization of *Xist* RNA. Dev Cell 19, 469–476.

Haustein E, Schwille P (2007). Fluorescence correlation spectroscopy: novel variations of an established technique. Annu Rev Biophys Biomol Struct 36, 151–169.

Heard E, Bickmore W (2007). The ins and outs of gene regulation and chromosome territory organisation. Curr Opin Cell Biol 19, 311–316.

Heard E, Disteche CM (2006). Dosage compensation in mammals: fine-tuning the expression of the X chromosome. Genes Dev 20, 1848–1867.

Heard E, Mongelard F, Arnaud D, Avner P (1999). *Xist* yeast artificial chromosome transgenes function as X-inactivation centers only in multicopy arrays and not as single copies. Mol Cell Biol 19, 3156–3166.

Helbig R, Fackelmayer FO (2003). Scaffold attachment factor A (SAF-A) is concentrated in inactive X chromosome territories through its RGG domain. Chromosoma 112, 173–182.

Herzing LB, Romer JT, Horn JM, Ashworth A (1997). *Xist* has properties of the X-chromosome inactivation centre. Nature 386, 272–275.

Janicki SM *et al.* (2004). From silencing to gene expression: real-time analysis in single cells. Cell 116, 683–698.

Jaramillo AM, Weil TT, Goodhouse J, Gavis ER, Schupbach T (2008). The dynamics of fluorescently labeled endogenous gurken mRNA in *Drosophila*. J Cell Sci 121, 887–894.

Khalil AM *et al.* (2009). Many human large intergenic noncoding RNAs associate with chromatin-modifying complexes and affect gene expression. Proc Natl Acad Sci USA 106, 11667–11672.

Lee JT, Strauss WM, Dausman JA, Jaenisch R (1996). A 450 kb transgene displays properties of the mammalian X-inactivation center. Cell 86, 83–94.

Lowary PT, Uhlenbeck OC (1987). An RNA mutation that increases the affinity of an RNA-protein interaction. Nucleic Acids Res 15, 10483–10493.

Lyon MF (2003). The Lyon and the LINE hypothesis. Semin Cell Dev Biol 14, 313–318.

Minks J, Brown CJ (2009). Getting to the center of X-chromosome inactivation: the role of transgenes. Biochem Cell Biol 87, 759–766.

Niwa H, Yamamura K, Miyazaki J (1991). Efficient selection for high-expression transfectants with a novel eukaryotic vector. Gene 108, 193–199.

Okamoto I, Otte AP, Allis CD, Reinberg D, Heard E (2004). Epigenetic dynamics of imprinted X inactivation during early mouse development. Science 303, 644–649.

Panning B, Dausman J, Jaenisch R (1997). X chromosome inactivation is mediated by *Xist* RNA stabilization. Cell 90, 907–916.

Payer B, Lee JT (2008). X chromosome dosage compensation: how mammals keep the balance. Annu Rev Genet 42, 733–772.

Ponting CP, Oliver PL, Reik W (2009). Evolution and functions of long noncoding RNAs. Cell 136, 629–641.

Popova BC, Tada T, Takagi N, Brockdorff N, Nesterova TB (2006). Attenuated spread of X-inactivation in an X;autosome translocation. Proc Natl Acad Sci USA 103, 7706–7711.

Pullirsch D, Hartel R, Kishimoto H, Leeb M, Steiner G, Wutz A (2010). The Trithorax group protein Ash2l and Saf-A are recruited to the inactive X chromosome at the onset of stable X inactivation. Development 137, 935–943.

Rabut G, Ellenberg J (2004). Automatic real-time three-dimensional cell tracking by fluorescence microscopy. J Microsc 216, 131–137.

Rinn JL *et al.* (2007). Functional demarcation of active and silent chromatin domains in human HOX loci by noncoding RNAs. Cell 129, 1311–1323.

Sado T, Hoki Y, Sasaki H (2005). *Tsix* silences *Xist* through modification of chromatin structure. Dev Cell 9, 159–165.

Sado T, Okano M, Li E, Sasaki H (2004). De novo DNA methylation is dispensable for the initiation and propagation of X chromosome inactivation. Development 131, 975–982.

Savarese F, Flahndorfer K, Jaenisch R, Busslinger M, Wutz A (2006). Hematopoietic precursor cells transiently reestablish permissiveness for X inactivation. Mol Cell Biol 26, 7167–7177.

Schoeftner S, Sengupta AK, Kubicek S, Mechtler K, Spahn L, Koseki H, Jenuwein T, Wutz A (2006). Recruitment of PRC1 function at the initiation of X inactivation independent of PRC2 and silencing. EMBO J 25, 3110–3122.

Seidl CI, Stricker SH, Barlow DP (2006). The imprinted Air ncRNA is an atypical RNAPII transcript that evades splicing and escapes nuclear export. EMBO J 25, 3565–3575.

Sun BK, Deaton AM, Lee JT (2006). A transient heterochromatic state in *Xist* preempts X inactivation choice without RNA stabilization. Mol Cell 21, 617–628.

Tang YA, Huntley D, Montana G, Cerase A, Nesterova TB, Brockdorff N (2010). Efficiency of *Xist*-mediated silencing on autosomes is linked to chromosomal domain organisation. Epigenetics Chromatin 3, 10.

Wutz A, Jaenisch R (2000). A shift from reversible to irreversible X inactivation is triggered during ES cell differentiation. Mol Cell 5, 695–705.

Wutz A, Rasmussen TP, Jaenisch R (2002). Chromosomal silencing and localization are mediated by different domains of *Xist* RNA. Nat Genet 30, 167–174.